Pergamon

Geochimica et Cosmochimica Acta, Vol. 68, No. 4, pp. 743–757, 2004

0016-7037/04 $30.00 + .00

doi:10.1016/S0016-7037(03)00488-5

The dynamics of cyanobacterial silicification: An infrared micro-spectroscopic investigation

LIANE G. BENNING,[1,*] V. R. PHOENIX,[2] N. YEE,[1] and K. O. KONHAUSER[1,†]

[1]School of Earth Sciences, University of Leeds, Leeds, LS2 9JT, UK
[2]Department of Geology, University of Toronto, Toronto, ON M5S 3B1, Canada

(*Received August* 6, 2002; *accepted in revised form April* 21, 2003)

Abstract—The dynamics of cyanobacterial silicification was investigated using synchrotron-based Fourier transform infrared micro-spectroscopy. The changes in exo-polymeric polysaccharide and silica vibrational characteristics of individual *Calothrix* sp. filaments was determined over time in a series of microcosms in which the microbially sorbed silica or silica and iron load was increased sequentially. The changes in intensity and integrated area of specific infrared spectral features were used to develop an empirical quantitative dynamic model and to derive silica load-dependent parameters for each quasi-equilibrium stage in the biomineralization process.

The degree of change in spectral features was derived from the increase in integrated area of the combined silica/polysaccharide region (Si-O/C-O, at 1150–950 cm^{-1}) and the Si-O band at 800 cm^{-1}, the latter representing specific silica bonds corresponding to hydrated amorphous SiO_4 tetrahedra. From the degree of change, a two-phase model with concurrent change in process was derived. In the first phase, a biologically controlled increase in thickness of the exo-polymeric polysaccharide sheath around the cell was observed. In phase two, a transition to an inorganically controlled accumulation of silica on the surface of the cyanobacterial cells was derived from the change in integrated area for the mixed Si-O/C-O spectral region. This second process is further corroborated by the synchronous formation of non-microbially associated inorganic SiO_4 units indicated by the growth of the singular Si-O band at 800 cm^{-1}. During silicification, silica accumulates (1) independently of the growth of the sheath polysaccharides and (2) via an increase in chain lengths of the silica polymers by expelling water from the siloxane bonds. IR evidence suggest that an inorganic, apparently surface catalyzed process, which leads to the accumulation of silica nanospheres on the cyanobacterial surfaces governs this second stage. In experiments where iron was present, the silicification followed similar pathways, but at low silica loads, the iron bound to the cell surfaces slightly enhanced the reaction dynamics.

1. INTRODUCTION

Silicification of microorganisms occurs in abundance in many hot spring environments where they are exposed to geothermal waters supersaturated with respect to amorphous (opal A) silica (Walter et al., 1972; Walter, 1976; Ferris et al., 1986; Schultze-Lam et al., 1995; Cady and Farmer, 1996; Hinman and Lindstrom, 1996; Konhauser and Ferris, 1996; Jones et al., 1998; Konhauser et al., 2001; Mountain et al., in press). Studies of microbial silicification are important as they not only provide insights into microbe-silica interactions in modern hot springs, but also because modern geothermal systems provide contemporary analogues for conditions under which some Precambrian microorganisms may have been fossilized (Konhauser, 2000; Cady, 2001; Toporski et al., 2002). Thus, a better understanding of the microbial silicification processes will enhance our knowledge about how microbes flourish in an environment subject to extensive silica precipitation and how they may become embedded in modern silica sinters or are preserved as microfossils.

The role microorganisms play in silica precipitation is currently not well defined. Many previous experimental studies have focused on the detail and quality of preservation of the microbes. In such studies, silicification was often induced with organosilicon solvents such as tetraethylorthosilicate (Leo and Barghoorn, 1976; Walters et al., 1977; Francis et al., 1978; Westall et al., 1995) and/or a variety of temperatures and/or pressures (e.g., 100–300°C and 1000–3000 bars [Oelher and Schopf 1971]; 70°C and 1 bar [Ferris et al., 1986]; 4–25°C and 1–500 bars [Westall et al., 1995; Toporski et al., 2002]). Although such studies provide significant insights into predominantly diagenetic related fossilization processes, they provide less insight into the mechanisms controlling microbial silicification in environments such as modern hot springs or the ancient oceans.

A series of field and laboratory based studies recently discussed silica precipitation in the presence of microorganisms (e.g., Cady and Farmer, 1996; Jones et al., 1999; Konhauser et al., 2001; Phoenix et al., 2001, in press; Mountain et al., in press; Yee et al., 2003). However, all these studies discuss bulk changes in solution or show microscopic evidence of extracellular silicification. In addition, most studies of metal uptake by microbial cells measure bulk changes in the experimental fluid and assume that the metals lost from solution were immobilized onto the cell surface (Fein et al., 1997; Daughney et al., 1998; Fowle et al., 2000). Such assumptions are pertinent for undersaturated systems. However, this approach becomes problematic when dealing with supersaturated systems (as is often the case with silica in geothermal systems). In natural as well as laboratory systems where supersaturated silica solutions are used, silica may nucleate homogeneously, or heterogeneously

* Author to whom correspondence should be addressed (l.benning@earth.leeds.ac.uk).
† *Present address:* Department of Earth and Atmospheric Sciences, University of Alberta, Canada.

onto the reaction vessel wall, or in solution. Under such conditions, bulk measurements of the experimental fluid will overestimate the amount of metal or silica immobilized by the microorganisms. Recent laboratory studies using batch sorption microcosms demonstrated that microbes have a low affinity for aqueous silica (Fein et al., 2002), even when they are placed in solutions supersaturated with respect to amorphous silica (Phoenix, 2001; Yee et al., 2003; Phoenix et al., in press). However, microscopic observations of field samples suggested that the silicification of microorganisms in modern hot springs occurs rapidly (e.g., Jones et al., 1998, 1999; Mountain et al., in press). Such rapid silicification may however, mainly point towards inorganic driving forces controlling the extensive microbial silicification observed in nature (i.e., cooling and evaporation of spring-water, which induces silica supersaturation and polymerization). Microscopic studies of hot spring silicified microorganisms have suggested that microbes may have acted as nucleation sites for silica precipitation (Schultze-Lam et al., 1995; Konhauser and Ferris, 1996; Jones et al., 1999; Mountain et al., in press), yet the controlling factors are unknown and direct proof of the microbial role in silica biomineralization is lacking.

Single-step batch microcosm experiments showed that silica immobilization by microbes is minimal (Fein et al., 2002; Yee et al., 2003; Phoenix et al., in press) and that the role microorganisms play in the silicification process may have been overestimated or misinterpreted in the microscopic observations. However, recent studies (Phoenix, 2001; Benning et al., 2003) have demonstrated that repeatedly exposing cyanobacteria to freshly prepared, supersaturated polymerizing silica solution by regularly replacing the experimental fluid (which could be envisaged as a pseudo flow-through system) can induce extensive biomineralization similar to that observed in hot springs. Furthermore, it has been shown that cyanobacteria continue to metabolize and function during extensive silicification (Phoenix et al., 2000). Such methods, although they did not provide any direct evidence about the processes controlling biomineralization, mimic the silicification reactions in hot springs more realistically and were therefore used as a basis to start the study presented here. Hence the use of a similar experimental protocol combined with the focussing capabilities of non-destructive, synchrotron-based Fourier transform infrared micro-spectroscopy, serves as a means for (1) the evaluation of the response (i.e., changes in cellular chemistry) of individual cyanobacterial filaments during silicification and (2) the evaluation of the extent and mechanism of silicification of individual filaments. This is in contrast to a generalized analysis of the microbial population's response as a whole to the average extent of silica removal, as derived from batch experiments. The effect an increasing silica load had on the organic components of individual cyanobacterial filaments was followed in situ and in vivo, via the changes in the infrared signature of single filaments. This approach allowed the quantification of the actual, and not the apparent, silica biomineralization process, and lead to the development of an empirical model that describes the processes controlling the biomineralization of cyanobacterial filaments. The differentiation between growth of the sheath in response to increasing silica load, and growth and aggregation of inorganic silica particles in response to an increasing silica load was possible, thus permitting a better interpretation of the roles of various cellular components in silica biomineralization.

2. EXPERIMENTAL PROCEDURES

2.1. Microbial Culture and Silicification Experiments

The filamentous cyanobacteria, *Calothrix* sp. (strain KC97), an isolate from the Krisuvik Hot Springs in Iceland (Phoenix, 2001) was used as a type strain. Cultures of *Calothrix* sp.—a relatively slow-growing cyanobacterial strain—were grown in autoclaved liquid BG11-N media (Rippka et al., 1979) at 28°C under an average cool white fluorescent light intensity of 24 μmol m^{-2} s^{-1}. After 4 weeks, a mature culture still in growth phase was obtained. For the silicification experiments identical cyanobacterial microcosms were prepared by gently homogenizing (to separate the filament clusters) and diluting with 18 MΩ water to an optical density of 0.75 at 720 nm. Subsequently, 5-mL aliquots were added to 50-mL polypropylene centrifuge tubes, centrifuged for 5 min at 3000*g* to pellet the cyanobacteria and the eluent then decanted off. Viability checks using phycoerythrin autofluorescence (this phycobilin is dispersed rapidly upon lysis) performed with a Nikon Microphot-FXA fluorescence microscope demonstrated that homogenization, dilution or subsequent centrifugation did not adversely affect cell viability. The biomass of a pellet obtained from a 5-mL aliquot was determined by filtering aliquots through 0.2-μm Supor filters and subsequently air drying at 70°C. This method provided a constant biomass of 2.3 mg of *Calothrix* sp. per microcosm.

Stock monomeric silica solutions (10.7 mmol/L, or 300 ppm as Si) were prepared from $Na_2SiO_3 \cdot 7H_2O$, and sterile 18 MΩ water. Immediately before addition to each microcosm, this solution was neutralized to pH $\sim$ 7 with a 2 mol/L HCl solution thus inducing silica polymerization. Various microcosms were prepared by adding 10 mL of this Si solution to the centrifuged pellet, which was subsequently re-suspended by vigorous shaking (experiments subsequently termed "Si"). To enable the cyanobacteria to metabolize and respond to silicification the silica stock solution also contained 10% BG11-N nutrient media. Parallel microcosms were prepared with the 10.7 mmol/L (300 ppm) Si solution spiked with 0.9 mmol/L (50 ppm) iron (made from ferrous chloride, experiments subsequently termed 'Si + Fe', Table 1). The addition of iron (an important nutrient) in the Si + Fe system did not enhance cell growth compared to the Si systems. This was because in both sets of experiments (Si and Si + Fe) enough iron (0.1 ppm) for cell metabolism was provided by the addition of BG11-N.

All microcosms were subsequently stored at 25°C under a cool white fluorescent low light intensity of 6 μmol m^{-2} s^{-1} to allow the cyanobacteria to photosynthesize and respond to silicification. Moderate temperatures and low light intensities were used to prevent significant multiplication of cell numbers during the experiment. After equilibration with the silica (or silica + iron) solution for 2 to 3 days, the solution was replaced with 10 mL of freshly prepared Si (or Si + Fe) solution. This solution replacement step was repeated for up to 12 times, and between each step, a 2- to 3-days equilibration period was allowed. During each step, 3.6 μmol (or 10 ppm) of Si were sorbed by the cyanobacterial surfaces (details of how this was determined are described in section 2.3, data in Table 1). Periods of longer than 2 to 3 d did not notably change the amount of sorbed silica, indicating that equilibrium had been reached, thus providing a linear relationship between the number of solution exchanges and the total sorbed silica.

Cyanobacterial control materials used in this study were *Calothrix* sp. whole-cells (i.e., filaments, which are intact 'chains' of cells surrounded by a exo-polymeric polysaccharide sheath), and chemically purified *Calothrix* sp. sheaths. For the silica control, the freshly polymerized silica or silica + iron stock solutions were used. The whole-cells used as control were prepared following the same steps as described above, but they were not silicified. For the sheath control, a purification method adapted after Weckesser et al. (1988) was used to isolate the sheath from the rest of the microorganism; a detailed description of the procedure can be found in Benning et al. (2003). As with the controls for the whole-cells, the purified sheath controls were not silicified.

Table 1. Experimental details for the silicification experiments. The (Si-x) runs represent the pure silica runs while the ones denoted (Si + Fe-x) represent the experiments where the silica solution was spiked with iron.

Sample	Number of solution changes[a]	Total equilibration time (h)	Total Si sorbed (μmol/microcosm)[b]	Total Si sorbed per bacterial mass (μmol Si/mg bacteria)[c]
Si-A	12	720	42.7	18.6
Si-B	9	552	32.0	14.0
Si-C	6	384	21.4	9.3
Si-D	3	216	10.7	4.6
Si-E	2	144	7.1	3.1
Si-F[d]	1	96	3.6	1.6
Si-G[d]	1	24	3.6	1.6
Si-Fe-A	12	720	42.7	18.6
Si-Fe-B	9	552	32.0	14.0
Si-Fe-C	6	384	21.4	9.3
Si-Fe-D	2	144	7.1	3.1
Si-Fe-E	1	96	3.6	1.6

[a] 3.6 μmol Si sorbed by the cyanobacterial biomass during each solution change.

[b] 3.6 μmol $\times$ number of changes.

[c] Biomass = 2.3 mg of bacteria per microcosm.

[d] The amount of sorbed silica on samples Si-F and Si-G are equal but the equilibration times are 24 h for Si-G and 96 h for Si-F; however, in terms of spectral features or intensities no difference was observed between the two samples.

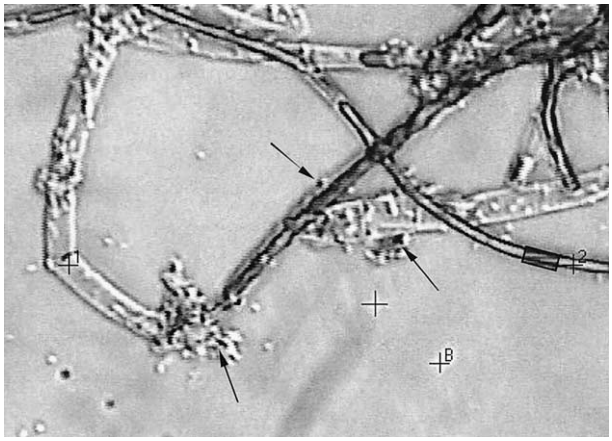

Fig. 1. Infrared bright field photomicrograph, showing a *Calothrix* sp. whole filament and its separated sheath. The picture was captured in visible light mode at 320$\times$ magnification. The size of the aperture (gray shaded box on a filament in the right lower corner) was set to 20 $\times$ 10 μm^2 and 'B' represents the point where the background was recorded. Note that measurements were only carried out on bacterial filaments or sheaths that were larger than or equal in size to the cutoff size set for all measurements (>90% of a 20 $\times$ 10 μm^2 aperture 'box' must be filled with sample). In addition, extreme care was taken to avoid cells or sheaths that were close to or had loose particles deposited on them (arrows).

2.2. Micro-Spectroscopy and Electron Microscopy

Before the infrared measurement, aliquots of each silicified sample were diluted, repeatedly washed by centrifugation in 18 MΩ water to remove any aqueous silica or non-attached silica particles, and dispersed using an ultrasonic disintegrator (Sanyo Soniprep 150, output frequency = 23 kHz, amplitude = 6 μm). During sonnication, most of the whole-cell filaments remained intact. However, some of the sheaths were mechanically separated from the silicified whole-cell filaments (Fig. 1). The occasional separation of sheaths from the filaments during the sonication process meant that FTIR spectra of such separated but silicified sheaths could be analyzed independently of the silicified whole-cells. In all discussions below, spectra of silicified whole-cells (intact filaments including sheaths; see section 3.3.1) or spectra of separated silicified sheaths (see section 3.3.2.) refer to analyses performed on these two fractions. Conversely, the control samples for the whole-cell and the chemically purified sheath were not silicified and only used for band assignments (see section 2.4).

From each suspension (both controls and silicified samples), 100 $\pm$ 2 μL were transferred onto 100% mid-IR reflectance slides (Kevley Technologies, USA) and dried in an incubator at 30°C for 4 h. Post-experimental culturing of cyanobacteria deposited on these slides showed that the cells were dehydrated but still viable. Repeat spectra collected on the same samples several months later still showed strong water peaks indicating that catastrophic dehydration of the cells had not occurred. This observation, along with the successful post IR-analysis culturing of cyanobacteria from the slides corroborated that the cells were still viable, thus confirming the non-destructive nature of the infrared radiation and the drying process.

The infrared measurements were carried out on station 13.3 at the Daresbury Laboratory, Warrington (UK) using a Nicolet NicPlan Infrared Microscope fitted with a 730 mid-IR spectrometer with the light derived from an external synchrotron source. The spectra were collected in reflectance mode with a liquid N_2 cooled mercury-cadmium-telluride (MCT) detector, at a resolution of 8 cm^{-1}, by co-adding and averaging 256 scans per point. A Happ-Genzel apodisation function was used, with the zero-filling factor set to two. A camera attached to the bright field microscope enabled optical imaging and recording of the investigated areas via the 32$\times$ Cassegrain objective (Fig. 1). Triplicate absorbance spectra over the range of 600 to 4000 cm^{-1} were collected in reflectance mode after the interferogram was checked for saturation. The measurements were carried out with the aperture on the microscope set so that the beam was focussed onto a 20 $\times$ 10 μm^2 area. Background spectra were collected on a sample-free area of the slide after every third sample spectra. The collected spectra were all processed using the Nicolet OMNIC and Atlμs software (ThermoNicolet Ltd.). Further details about the method are given in Benning et al. (2003).

Control (unsilicified) and silicified cyanobacteria and sheaths from each batch deposited on the IR reflective sides were examined using a field emission scanning electron microscope (FEG-SEM, LEO 1530). Aliquots of the samples prepared for the IR measurements were deposited on stubs and dried under sterile conditions in a laminar flow hood for 4 h. These samples were subsequently coated with a 2-nm platinum layer and examined at 1 to 3 keV at a working distance of 2 to 4 mm and using the in-lens secondary electron detector.

2.3. Silica Sorption Computation

The data analysis presented below exploits the change in FTIR absorbance to derive coefficients related to the biomineralization process as a function of increasing silica load. The amounts of silica sorbed by the 2.3-mg biomass in each microcosm were evaluated from previously performed experiments (Phoenix, 2001) where identical experiments to those discussed here were carried out (i.e., 2.3 mg *Calothrix* biomass reacted with 10 mL of Si stock solution). To follow the silica removal by the biomass the amount of total non-sorbed silica (Si_{total}) remaining in solution was monitored at regular intervals between 0 and 400 h by Inductively Coupled Plasma Atomic Emission Spectrometry (ICP-AES). Concurrently, blank runs (with silica but no cyanobacteria) were carried out to correct for silica that precipitated from the aqueous fraction by inorganic polymerization (Si_{blank}), and which was not immobilized by the cyanobacterial biomass (i.e., inorganic precipitation). The data plotted in Figure 2 shows one such experiment where from an initial 293 ppm Si (equivalent to 105 μmol of Si in the 10 mL of reacting solution), only 4 μmol of Si ($\sim$10 $\pm$ 0.6 ppm Si) were immobilized by the cyanobacterial biomass (Si_{sorbed}) after 72 h. Triplicate measurements revealed an average of 3.6 $\pm$ 0.6 μmol of Si immobilizaed by the cyanobacterial fraction, which represents < 4% of

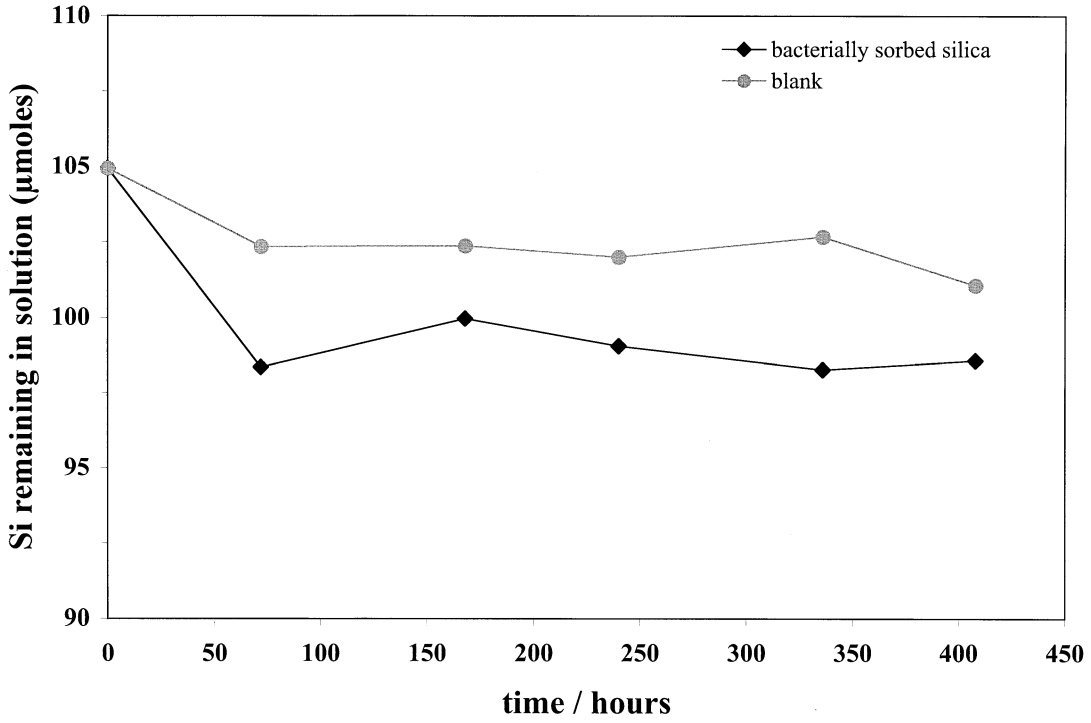

Fig. 2. Removal of silica (plotted as Si remaining in solution) over ~400 h in an experiment with an initial 105 μmol of Si in the 10 mL solution (corresponds to an initial 293 ppm Si) and in the presence of 2.3 mg biomass (black diamonds) or in the blank (gray circles).

the total silica in solution. Furthermore, experiments carried out for < 100 h (data not shown, Phoenix, 2001), have demonstrated that most of the cyanobacterial Si immobilization (~95%) actually occurred within the first 12 h, with negligible Si sorption occurring after that. In the present study, the silica and silica + iron solutions were replaced every 2 to 3 days with a maximum of 12 solution changes. Therefore, with 3.6 μmol Si immobilized by the cyanobacterial biomass during each 2- to 3-day step, a maximum Si-load of ~43 μmol of sorbed silica was reached (Table 1). The total Si accumulation in the mixed Si + Fe experiments was derived from mixed Si + Fe batch microcosms (Phoenix, 2001). Although the addition of Fe increased the total aqueous silica removal, most of this was due to inorganic flocculation (that was also present in the blank) and therefore ~4 μmol Si (per solution change) were again estimated to be sorbed by the cyanobacterial biomass. This relationship allowed the quantification of the dynamics of silica accumulation on the cyanobacterial cells as a function of total sorbed silica. The results of these calculations and further details for the silicification experiments are shown in Table 1.

In all experiments presented here, *time* (the usual parameter used in kinetic-type quantifications) is not a meaningful parameter as the microcosms were left in contact with the reacting solution far beyond the time when the equilibrium level of ~4 μmol sorbed Si was reached. However, using a mathematical approach similar to the one used in kinetic evaluations, allowed the derivation of a quantitative empirical model for the dynamics of silica accumulation. In the model presented here (section 4), the quantification of the silica accumulation coefficients relies on the increase in Si-load on the given biomass and thus the accumulation coefficients were expressed as Si-load dependent functions.

2.4. Spectral Corrections and Band Assignments

All background corrected reflectance spectra were transformed into absorbance spectra ($A = \log [1/R]$) using the Nicolet OMNIC and Atlμs software (ThermoNicolet Ltd.) and are presented as absorbance vs. wavenumber (cm^{-1}) plots. All spectra were baseline corrected for a desired frequency region. The control materials were used solely for frequency assignment purposes and thus the full spectral region was baseline corrected (4000–700 cm^{-1}). On the other hand, for the quantification of the microbial silicification dynamics, only vibrations in the frequency region between 1800 and 700 cm^{-1} were used because this region contains the most important microbial vibrations (the "double bond" and the "fingerprint" region; Diem, 1993; Stuart and Ando, 1997). Therefore, all silicified sample spectra were baseline corrected for this spectral region. All baseline corrections were done using the automatic baseline correction algorithm within the OMNIC software (the baseline set as a two-point straight-line between two end-points). This allowed a minimization of the differences between spectra due to baseline shifts and together with the background corrections, accounts for the effect of the intensity decay of the synchrotron beam.

The spectral band assignments in the control materials were derived by comparison and cross-referencing against literature data on other microbial cells, amorphous silica, or other macromolecules (Table 2, Fig. 3). At high wavenumbers, specific features for silica (band 1), OH (band 2) and lipids (region 3) were found. For the cyanobacterial whole-cells, the most characteristic features are the strong amide I and amide II bands (bands 5 and 6; C=O, 1650 cm^{-1} and N-H/C-N, 1540 cm^{-1}). In addition, less well-defined features from lipids (band 4, >C=O of membrane lipids, 1740 cm^{-1}; band 7, δ_{as} CH_2/δ_{as} CH_3 of lipids, 1450 cm^{-1}), carboxylic acid (band 8, C-O, 1392 cm^{-1}), nucleic acid or phosphorylated polysaccharides (band 9, P=O, 1245 cm^{-1}) and exo-polymeric polysaccharides (band 10, C-O, 1200–1000 cm^{-1}) are found. In contrast, the spectra for the purified sheath featured strong exo-polymeric polysaccharide vibrations (region 10, C-O, main peaks at 1165, 1110, 1050, and 1030 cm^{-1}) and weak amide, carboxylic acid and nucleic acid contributions from remnant cell material. From the spectra for the silica control, the main siloxane and silane frequencies are found between 1200 and 950 cm^{-1} (region 10, Si-O at 1190 cm^{-1}, a shoulder at 1115 cm^{-1}, and the main peak at 1060 cm^{-1}). These silica bands partially overlap with the exo-polymeric polysaccharide frequencies, making an accurate band assignment in this region difficult. However, at lower frequencies, two exclusive silica vibrations

Table 2. Frequencies and band assignments for characteristic vibrations found in the IR spectra of the *Calothrix* sp. whole-cells, chemically separated *Calothrix* sp. sheaths, and the silica controls.

Band #	Wavenumbers (cm^{-1})	Range[a] (cm^{-1})	Assignments[b] and main functional groups[c]
1	3750		Si-OH, surface hydroxyls
2	3300–3400		ν O-H and ν N-H of water and amide A
3	2960–2875		ν_{as} CH_3, ν_{as} CH_2, ν_s $>CH_2$/-CH_3; methyl and methylene groups of lipids
4	1740		ν >C=O of esters; membrane lipids
5	1650		ν C=O; amide I
6	1531[d]	1560–1470[d]	δ N-H and ν C-N; amide II
7	1450		δ_{as} CH_2/δ_{as} CH_3; lipids, amide III
8	1392		ν_s C-O; carboxylic acid
9	1245		ν_{as} P=O; nucleic acid, phosphorylated sugars
10	1200–950[e]	1150–950	ν C-O/ν Si-O; carbohydrates/ siloxanes
11	950		ν Si-OH; silanes/silanols
12	800	830–770	ν Si-O/SiO_4 rings/siloxane

[a] Range used for kinetics evaluations.
[b] ν = stretching; δ = bending; as = asymmetric, s = symmetric.
[c] Sources see Table 1 in Benning et al. (2003).
[d] Value or band used for normalization.
[e] Range of overlapping carbohydrate/silica frequencies.

(band 11, Si-OH at 950 cm^{-1} and band 12, Si-O at 800 cm^{-1}) which do not interfere with the organic vibrations in the *Calothrix* sp. whole-cells or sheath are found. Extensive details and discussions on all these vibrations and their characteristics can be found Benning et al. (2003).

3. RESULTS AND DATA ANALYSIS

3.1. Microscopic Evidence

FEG-SEM examinations of the control and of the silicified cyanobacteria showed that at low Si-load (~4 μmol sorbed Si) the cells remained relatively free of silica (Fig. 4a). However, cells exposed repeatedly to supersaturated and polymerizing silica solutions became encrusted in a matrix made up of 20- to ~200-nm silica spheres (Fig. 4b). In Figure 4b, shown are silica nano-spheres deposited on the sheath of a cyanobacterial filament that no longer contains the original cells. The FEG-SEM evidence indicates that this sheath was probably silicified while still enveloping a viable cell, because the original structure and morphology were retained even after lysis, suggesting prelysis encrustation. The sheath material may have been mechanically removed from the trichomes when colonies were sonnicated before IR measurements. Alternatively, separation of the sheath from the cell maybe a consequence of natural lysis occurring to a certain degree in all mature cultures of *Calothrix* sp. (no colony is 100% viable and the sheaths tend to persist after the lysed cells have dispersed). However, if the separation between sheath and cell occurred before silicification it would

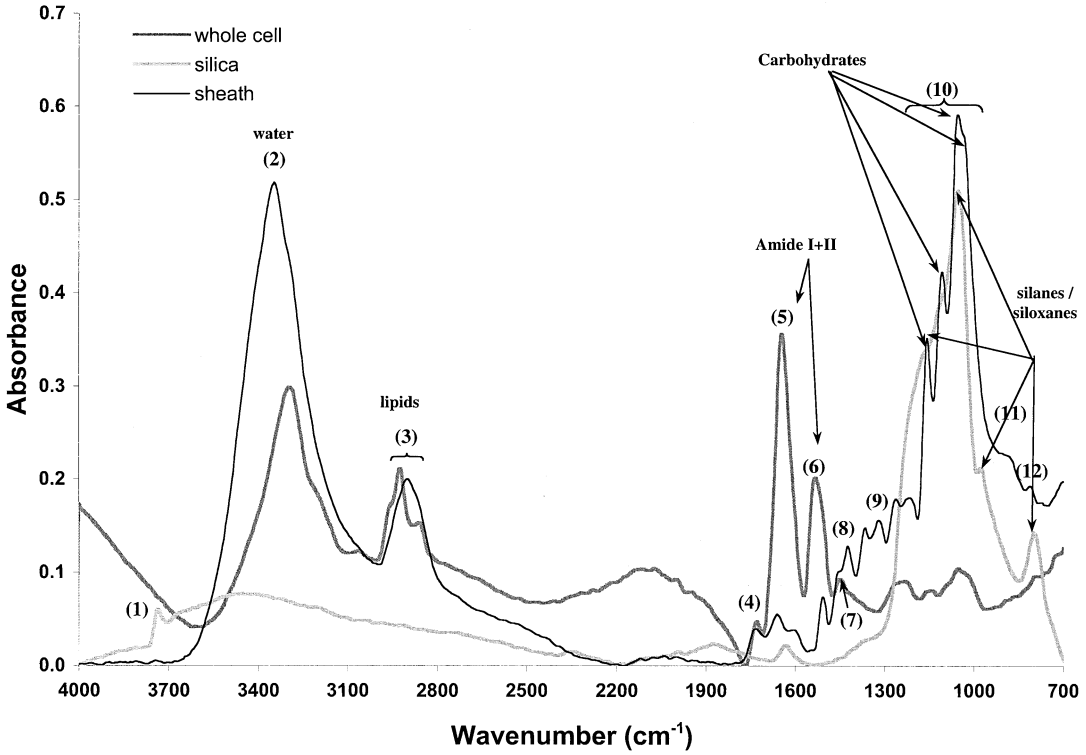

Fig. 3. Representative FTIR absorbance spectra for the controls used for spectral assignment: *Calothrix* sp. whole cell, chemically separated *Calothrix* sp. sheath and the silica control. All spectra were baseline corrected for frequencies between 4000 and 700 cm^{-1} and the details for the band assignments are discussed in the text and in Benning et al. (2003). Numbers in brackets correspond to the band # in Table 2 and main functional groups are shown above the specific band or indicated by arrows.

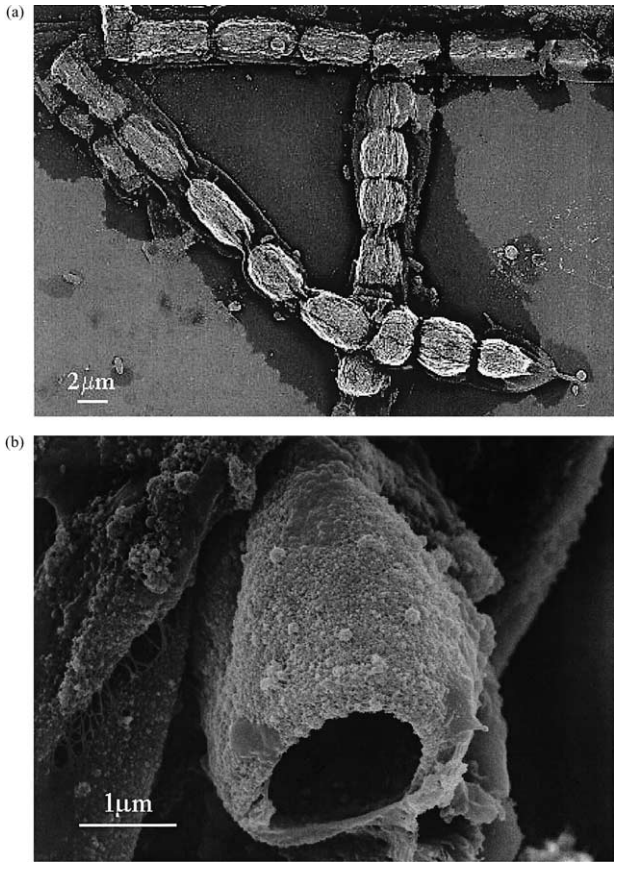

Fig. 4. FEG-SEM photomicrograph of *Calothrix* sp. with increasing Si-load. (a) Cells from experiment Si-G with an estimated 3.6 μmol Si sorbed. The filaments are made of cells of about 2 to 4 μm in length that are enclosed by a thin polysaccharide sheath. (b) Heavily silicified empty sheath from experiment Si-A, with an estimated Si-load of 43 μmol Si. Note that the sheath is covered with 20- to 200-nm silica spheres.

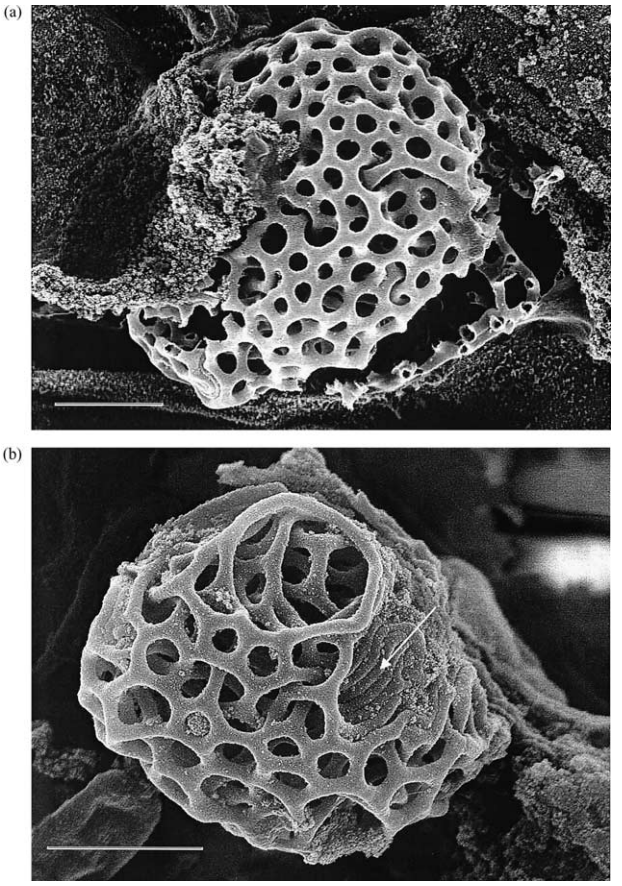

Fig. 5. FEG-SEM photomicrograph of silica structures observed in the most silicified sample (Si-load = 43 μmol). (a) A mesh-like interconnected empty skeleton of hollow tubes of $\leq$ 100 nm diameter that are configured in a pentagonal framework. (b) Structure similar to (a) but also visible is a close-winding arrangement—see arrow—and 20- to 50-nm particles scattered on the mesh; samples were coated with 2 nm platinum; scale bar in both photographs is 1μm.

not be expected to have the morphology of the cell retained, as undoubtedly the sheath would have collapsed.

One additional interesting observation was made in the most silicified sample (at 43 μmol sorbed silica). In this sample, seemingly self-organized structures made of pure silica (confirmed with EDS point measurements) resembling radiolarian or diatomaceous structures were observed (Fig. 5). These structures, which are not cyanobacterial in origin, resemble hexagonal siliceous diatomaceous cell walls (frustules) which have been shown to use amphiphilic methylated polypeptides to create their intricate nano-pattern (Kröger et al., 1997, 2000; Sumper, 2002). However, the tubular structures described here (1) were at least an order of magnitude smaller than those in diatoms (scale in Fig. 5 is 1 μm) and (2) the mesh that makes up these structures was braided and not planar. The mesh was made up of intricately intertwined hollow tubes with diameters of $<$ 100 nm (Fig. 5a) that were arranged in an array of irregular pentagonal or hexagonal coordination (although in one case also a closely winding configuration was observed; arrow in Fig. 5b). These structures are very similar in size and organizational patterns to self-assembled silica nano-tubes and wires (e.g., Whitesides and Grzybowski, 2002) formed via organic peptides or polyamide paths (Cha et al., 2000; Lehn, 2002). In the experiments discussed here, those nano-tube-like configurations may have formed as a consequence of lysing of cells with subsequent reaction between the released cytoplasmic peptides/amides (up to 100 mmol/L; Diem, 1993) and the silica solution. Note also, that on the surface of the intertwined tubes, additional much smaller silica nanoparticles (20–50 nm in size, Fig. 5b) are visible. These small particles precipitated on the tubular structures and on the matrix and thus indicate their late stage formation. However, the process leading to the formation of these nano-tubes remains unclear as no infrared measurements on these structures are available.

3.2. Spectral Normalisation

In all spectra collected during the course of the silicification experiments several vibrational features showed distinct degrees of change with increasing Si-load. The vibrational bands with the most prominent increase in absorbance were band 10 and band 12 (Table 2). To quantify these changes and to correct

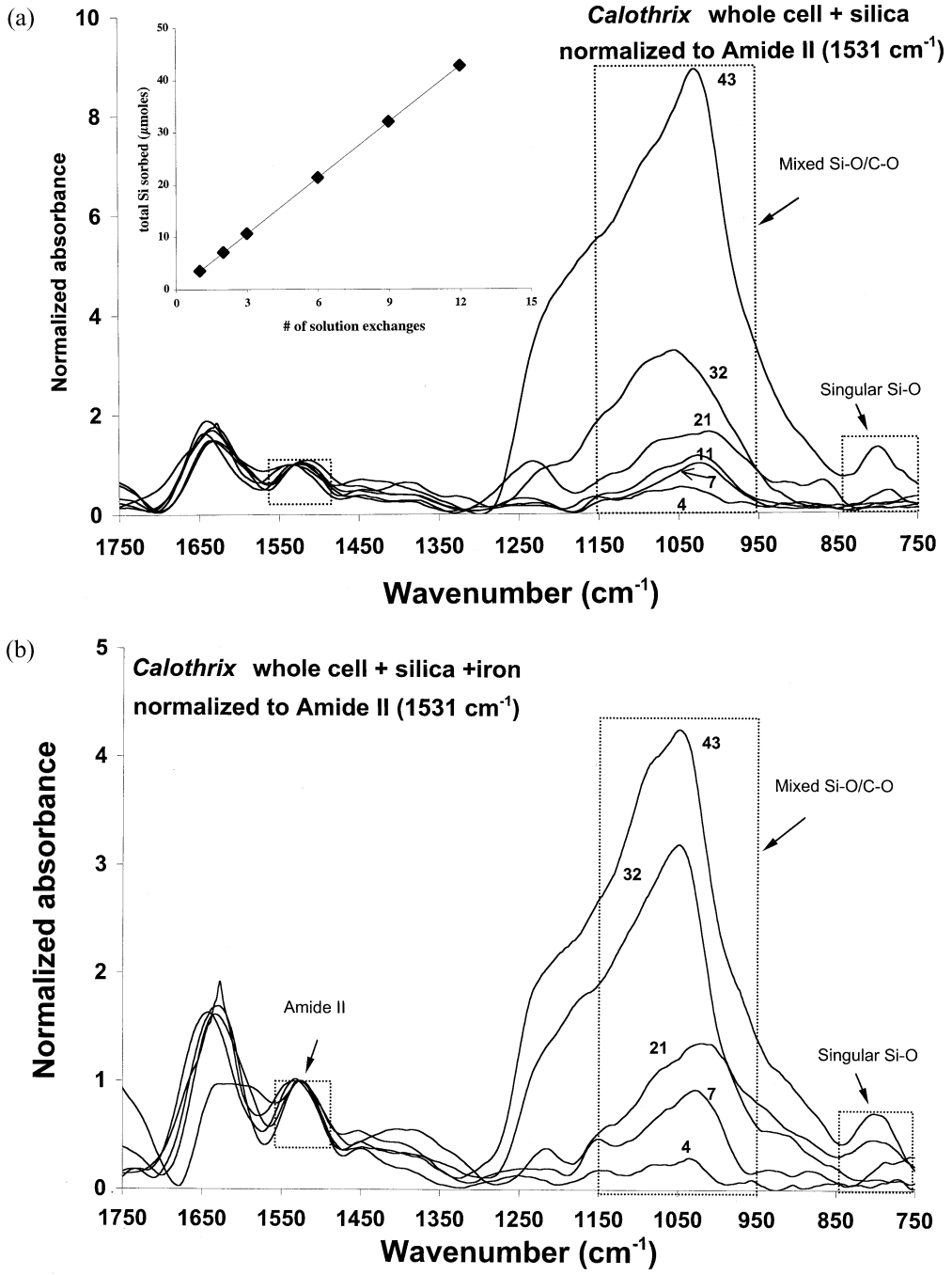

Fig. 6. Infrared absorbance spectra of progressively silicified *Calothrix* sp. whole-cells. All spectra were baseline corrected between 1800 and 700 cm^{-1} and normalized against the amide II peak at 1531 cm^{-1}. (a) Spectra for the whole-cells in the Si experiments. (b) Spectra for the whole-cells in the Si + Fe experiments. Inset in (a) shows the first order relationship between Si-load and # of exchange steps. The numbers next to the spectra correspond to total sorbed Si (in μmol) and the dotted boxes denote the frequency regions used for kinetic evaluations. Small dotted box at ~1500 cm^{-1} corresponds to the amide II band, the tall dotted box with the maximum at ~1050 cm^{-1} corresponds to band 10, the mixed Si-O/C-O band and the small dotted box at ~800 cm^{-1} corresponds to band 12, the singular Si-O band (see also Table 2).

for possible variations in path-length (thickness of individual cyanobacterial filaments or sheath) and water content, two normalization approaches were tested. First, the maximum absorbance intensities in the whole-cell spectra for band 10 and 12 (at 1049 and 802 cm^{-1}; Figs. 6a and 6b) were normalized to the maximum amide II absorbance band intensity (frequency at 1531 cm^{-1} = 1). This type of normalization gives an overview of the changes with increasing Si-load (Figs. 6a and 6b). These normalized maximum values were used to compute the change for the two bands (mixed Si-O/C-O band

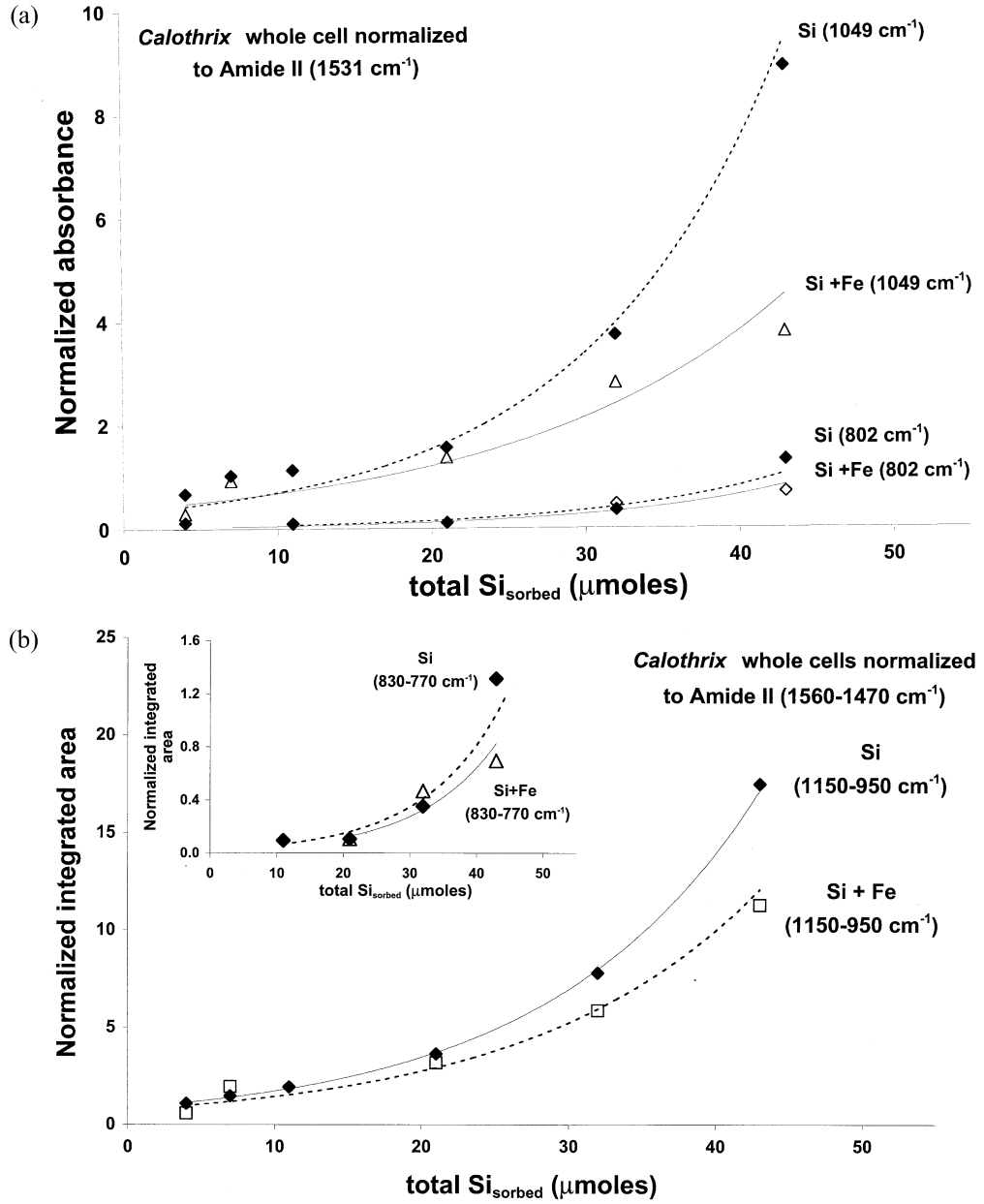

Fig. 7. Increase in absorbance intensity (normalized against amide II at 1531 cm^{-1}) or integrated area (normalized against amide II between 1560 and 1470 cm^{-1}) with increasing Si-load for both experimental sets (Si and Si + Fe). (a) Normalized absorbance intensity for the mixed Si-O/C-O peak at 1049 cm^{-1} (band 10) and the 802-cm^{-1} peak (band 12). (b) Normalized integrated area for the 1150 to 950 cm^{-1} region and the 830 to 770 cm^{-1} region.

10 and singular Si-O band 12) and for both sets of experiments (Si and Si + Fe) for the silicified whole-cells as a function of increasing Si-load (Fig. 7a). However, due to the variations in absolute vibrational frequencies and the overlap of silica and polysaccharide bands, it was more appropriate to use an integrated area-based normalization for the quantitative analyses. In this way, the integrated areas under bands 10 (between 1150 and 950 cm^{-1}) and 12 (between 830 and 770 cm^{-1}) were normalized to the area under the amide II band 6 (1560–1470 cm^{-1}). The area under these peaks was calculated by setting a window to bracket the desired region, with the area being the surface bordered by the spectrum and a baseline connecting set frequency limits on either side of the region of interest. The computed changes in integrated area for both regions of interest and for both sets of whole-cell spectra (Si and Si + Fe experiments) are plotted with increasing Si-load in Figure 7b. The amide II band is very characteristic and constant in all studied cells, and shows no interference with other vibrations and thus is ideal for normalization purposes. The spectra of the progressively silicified sheaths (i.e., the separated sheath found amongst the whole filaments, e.g., Figs. 1 and 4b) were not normalized because the protein content in the separated sheath varied and thus these bands were not constant in relative absorbance. Therefore, changes in the silicified sheath spectra

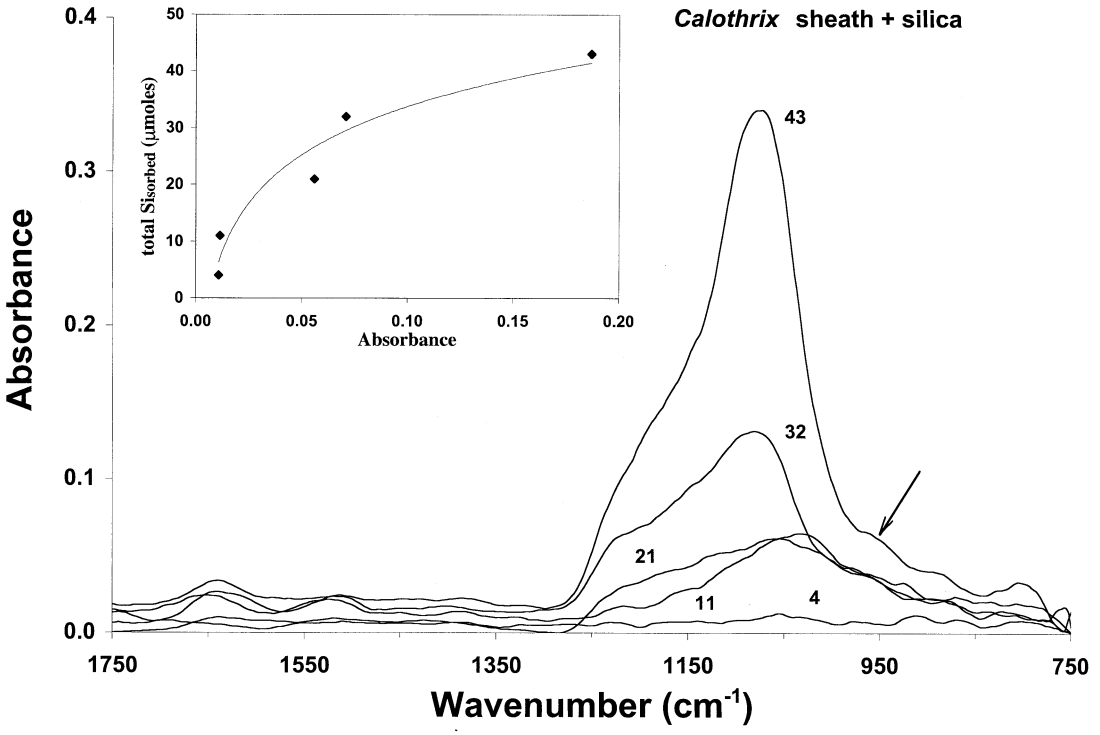

Fig. 8. Si-load-dependent spectra for the *Calothrix* sheaths in the Si experiments; the numbers next to the spectra correspond to total sorbed Si in micromoles; arrow indicates the appearance of the 950-cm^{-1} band. Inset shows the change in relative intensity of the mixed Si-O/C-O peak at 1050 cm^{-1}, with increasing Si-load (μmol).

were used only for comparison purposes and not for a quantitative evaluation (Fig. 8).

3.3. Changes in Infrared Spectra of Silicified Samples (Si and Si + Fe Experiments)

The effect pure silica or iron-doped silica solutions have on the *Calothrix* sp. filaments were quantified from the very characteristic changes observed in FTIR spectra of the progressively silicificed cyanobacteria (Figs. 6 and 7). To evaluate the experimental error in the infrared measurements, spectra of cyanobacteria from the same microcosm, spectra on the same cyanobacterial filament but on a different position along the filament, and spectra on the same spot were recorded. The measurements showed a high degree of reproducibility, indicating that in the same microcosm the variations between chosen filaments (in terms of thickness, biochemical signal, and water content) were minimal (see Fig. 3 in Benning et al., 2003). Reproducibility was also improved by selecting filaments and separated sheaths that were similar in size and appearance, and visibly free of loose particles (arrows in Fig. 1). Furthermore, spectra from samples at equal Si-load but that had been equilibrated with the supersaturated silica solution for different amounts of time (1 and 4 d, Si-F and Si-G in Table 1) were compared and showed equal relative absorbance intensities over the whole spectral region (data not shown).

3.3.1. Whole-Cells

The changes in normalized absorbance intensity (amide II at 1531 cm^{-1}=1) for whole-cell samples with progressive silicification (Si-experiments) are shown in Figure 6a, while the normalized spectra from the mixed Si + Fe experiments are shown in Figure 6b. The inset in Figure 6a applies to both experimental sets (Si and Si + Fe) and shows the first order relationship between the cumulative cyanobacterially-sorbed Si-load (see section 2.3) and the number of solution exchanges. In both sets of spectra, the absorbance intensity between ~1200 and 900 cm^{-1} increases with increasing Si-load. In the Si experiments (Fig. 6a), at the highest estimated Si-load (43 μmol) the maximum peak was found at 1030 cm^{-1} and this peak increased in intensity by 95% with respect to the initial spectrum at 4 μmol. Similarly, in the Si + Fe experiments (Fig. 6b) the change in maximum absorbance between the first (4 μmol) and the last spectrum (43 μmol) is 92% but the maximum peak shifted to slightly higher wavenumbers (maximum at 1055 cm^{-1}). In both sets, at a similar pace, the phosphodiester band (P=O at ~1240 cm^{-1}) and the first polysaccharide band (C-O at 1165 cm^{-1}) transformed into a broad shoulder of the main mixed Si-O/C-O band (1060–1030 cm^{-1}) which developed a steeper slope with increasing Si-load. In addition, with increasing Si-load the formation of a new band at ~800 cm^{-1} was observed. This latter band represents the Si-O stretching vibrations of the SiO_4 ring structure, and exhibited no interference with exo-polymeric polysaccharide groups of the cyanobacterial cell.

When comparing the normalized relative absorbance values of the Si + Fe experiments with the Si-experiments (Fig. 7a), notably smaller (~54%) maximum absorbancies were observed in the iron-doped experiments. The differences are diminished with decreasing Si-load and are most prominent in the

Si-O/C-O vibration (band 10, at 1049 cm^{-1}). At 32 μmol total sorbed Si, the maximum absorbance intensity in the Si + Fe experiments was 25% smaller than in the Si experiments (this difference was 12% at 21 μmol, and 8% at 7 μmol; Fig. 7a). A comparable but more quantitative measure for this difference was obtained when the normalized integrated areas for these two experimental sets were compared. The difference in normalized integrated areas for the two regions (1150–950 and 830–770 cm^{-1}) decreased with decreasing Si-load (Fig. 7b and inset). For the Si-experiments, the difference for the mixed Si-O/C-O area decreased from 35% at 43 μmol, to 22% at 32 μmol, 13% at 21 μmol and 2% at 7 μmol (Fig. 7b).

3.3.2. Sheaths

In the same samples and at the same Si-loads, spectra of silicified separated cyanobacterial sheath fragments (see Fig. 1) were also collected (this sheath material should not be confused with the chemical purified sheaths that were used as controls for band assignment). In Figure 8, the absorbance spectra for progressively silicified sheath samples for the Si-experiments are shown. These spectra were not normalized due to the lack of a protein or other molecules that could serve as a constant intensity identifier. No measurements are available for the Si + Fe experiments. The spectral quality and absorbance intensities in the silicified sheath spectra when compared with the silicified whole-cells were on average noisier and gave 30 to 50% lower relative absorbance intensity. This is mainly due to the fact that the sheaths are much thinner (i.e., shorter path-length, max. 2 $\times$ 0.02–0.5 μm) than the whole-cell (path-length = ~8–10 μm). The changes in the absorbance intensity of the mixed Si-O/C-O peak at 1050 cm^{-1} (band 10) were computed with increasing Si-load following a similar procedure as described for the whole-cell and are plotted in the inset in Figure 8. The comparison between silicified whole-cells and sheaths (Figs. 6a and 8) showed a comparable trend with the most noticeable change occurring again in the mixed Si-O/C-O vibrations (band 10). In absolute terms, with increasing Si-load (from 4–43 μmol), this band increased in absorbance intensity by 75% (Fig. 8), while at equivalent Si-loads the change in absorbance intensity in the whole-cell spectra (Fig. 6a) corresponded to a 95% increase. In the sheath spectra the two silica specific vibrations (950 and 800 cm^{-1}, bands 11 and 12) became more prominent at high Si-loads. The weak 950-cm^{-1} vibration was observed in the silicified sheath (arrow in Fig. 8) but not in the whole-cell spectra (Fig. 6) where it is hidden in the shoulder of the main peak. Due to the lack of an adequate vibration that could be used for normalization purposes, the observed changes in the silicified sheath were used to confirm the trends observed in the whole-cells spectra and to endorse the observed strong link between the growth of the cyanobacterial sheath (exo-polymeric polysaccharides) and silica precipitation but not for further quantitative assessment.

4. DISCUSSION

In active geothermal systems, the effluent solutions are often highly supersaturated with respect to amorphous silica (up to 2 orders of magnitude) and usually upon cooling spontaneous polycondensation of monosilicic acid, $Si(OH)_4$ is induced. It has been proposed that microorganisms may affect the polycondensation process by providing nucleation sited and thus lowering the interfacial free energy barriers required for precipitation. Amorphous silica is a non-stoichiometric inorganic polymer made up of a mixture of SiO_2 and H_2O units at various ratios. At the conditions of the experiments presented here the monomeric silanol groups (Si-OH) should spontaneously polymerize by condensation to form polysilicic acid oligomers of various lengths (dimers, trimers) that are bound together via siloxane bonds (Si-O-Si). These oligomers further aggregate to form 2- to 3-dimensional structures (e.g., Perry, 1989), leading to the formation of nano-particles that have often been observed to coat microorganisms in geothermal systems. However, the mechanisms that drive these processes are not well understood. Furthermore, although experimental evidence showed that upon silicification, *Calothrix* sp. produces a thicker exo-polymeric polysaccharide sheath (Phoenix et al., 2000), the mechanisms driving this process are unknown. It is known that the sheath of *Calothrix* sp. is composed mostly of glucose (Weckesser et al., 1988) and usually these 'sugar' polymers form linear polymer chains (Rees, 1977), however, their interaction with the polymerizing silica units was unclear.

The FTIR data presented above clearly show that the intensity or integrated area for the absorbance bands between 750 and 1300 cm^{-1} increases considerably with increasing Si-load. This increase can be primarily related to the formation of (1) more exo-polymeric polysaccharides and (2) the accumulation of silica oligomers and 3-dimensional silica nanoparticles on the cyanobacterial surfaces. Furthermore, the observed change can also be related to an increase in ionic character of the observed bonds. In abiotic experiments, it has been unambiguously shown that FTIR absorbance intensities of progressively deposited thin silica layers or thin films (Licoppe et al., 1992; Schwerha et al., 2002) or of hydrogenated amorphous silica films (Kessels et al., 2001) show a linear relationship to layer/film thickness. In the experiments presented here, the relationship between increasing Si-load and normalized integrated area reveals however, a polynomial relationship (Fig. 7b). This relationship indicates that the increase in normalized area for the mixed Si-O/C-O or the singular Si-O vibrations is a function of the increase in number of formed polysaccharide or SiO_4 units but also depends on the ionic character of the formed bonds. This change in bonding indicates a change in the process the mechanisms that controls the biomineralization of the cyanobacteria.

4.1. Theoretical Approach

Usually infrared data are quantified using the Beer-Lambert law (Stuart and Ando, 1997). However, because this study deals with a mixed system (cyanobacteria/silica), this approach could not be used as the molar absorbtivity values for the *Calothrix* sp. and for hydrated amorphous silica are poorly defined. It is well established that the growth and aggregation of polymers in solution (and of silica in particular) is strongly affected by pH, ionic strength, temperature and surfactant concentration and type (Rothbaum and Wilson, 1977; Iler, 1979, 1980; Makrides et al., 1980; Weres et al., 1981; Perry, 1989). Furthermore, it has been shown that inorganic silica precipitation usually occurs via a reaction-limited process (e.g., Rimstid

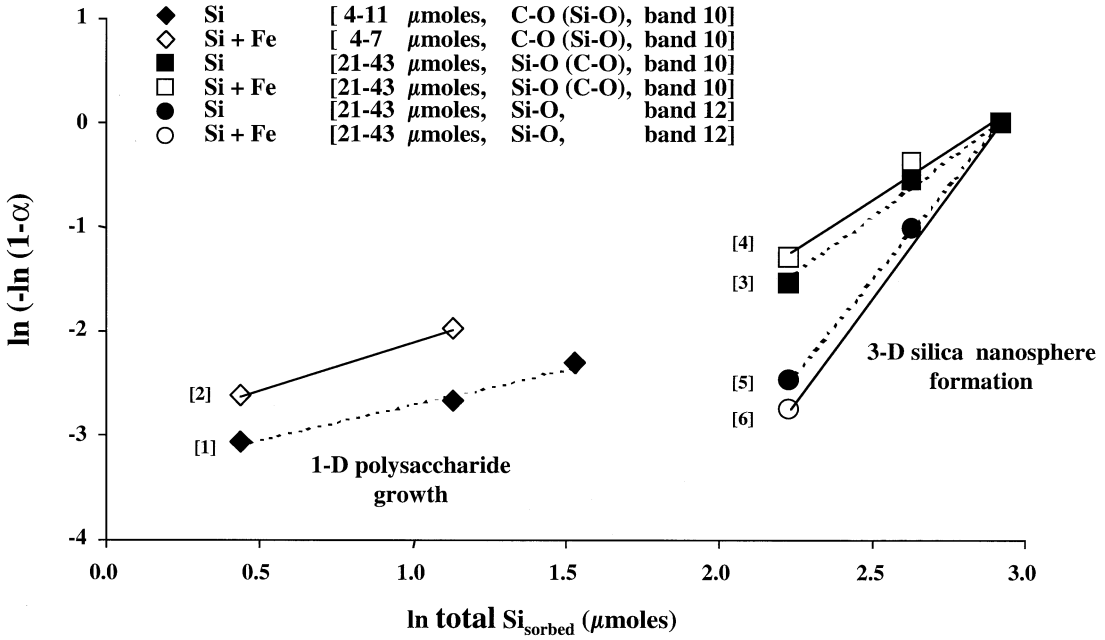

Fig. 9. Double logarithmic plot showing the change in aggregation mechanisms as derived from the normalized integrated areas of the mixed Si-O/C-O and the singular Si-O regions (bands 10 and 12) in the Si and Si + Fe experiments. The numbers in brackets next to each line correspond to the numbers in Table 3 that lists the k_a and n values for each fitted set.

and Barnes, 1980; Caroll et al., 1998). However, when kinetic rates are derived, 'time' is the commonly used rate dependent parameter. In this study, classical time-dependent reaction rates per se were not derived but only dynamic, silica load-dependent reaction parameters. These parameters refer to the changes observed in infrared features of the polysaccharide and silica bonds with increasing Si-load.

The degree of change was calculated from the integrated area ratio between the amide II band (1560–1470 cm^{-1}) and the main silica/polysaccharide region (1150–950 cm^{-1}) or the singular silica band at 830–770 cm^{-1}. The reaction progress (α) was calculated by setting

$$\alpha(x) = 1 - \frac{I(x)}{I(\infty)} \quad (1)$$

where $\alpha(x)$ is the fraction of the reaction completed at Si-load (x), I is the ratio between the integrated area of the peak of interest and the integrated area of the amide II peak ($I = \frac{I_{PoI}}{I_{AmII}}$), and $I(x)$ and $I(\alpha)$ are the integrated ratios at any Si-load and at maximum Si-load, respectively. This approach was employed as it reflects the fact that in these experiments silica accumulation is an ongoing process and the maximum Si-load reached was solely dependent on the number of solution exchanges that each microcosm was submitted to (Table 1). Although these experiments mimicked a pseudo-flow-through system, the Si-load at each step represented an equilibrium value. Values for $\alpha(x)$ for each step were derived from the above mentioned normalization and then subsequently fitted to an equation modified from the classical kinetic relation of Avrami (1941) but expressed as a function of Si-load:

$$\alpha(x) = 1 - \exp(-k_a x^n) \quad (2)$$

where k_a may be regarded as a proxy for the silica load-dependent reaction coefficient and n can be envisaged as a mechanism related constant. The values for the constants (k_a and n) in Eqn. 2 can be calculated after taking the double logarithm of this equation and using a least-squares regression for the equation:

$$\ln[-\ln(1-\alpha)] = n \ln k_a + n \ln x \quad (3)$$

A plot ($\ln[-\ln(1-\alpha)]$ vs. $[\ln x]$) corresponding to Eqn. 3 provides a straight line and the slope and intercept can be used to derive values for (n) and (k_a) respectively. However, in this model the values for n and k_a, can not be compared with similar parameters derived from kinetic data, as they do not have the same direct physical meaning. Therefore, the change in slope (n) could only be used to infer a change in process during the biomineralization experiments and could not be related directly to a mechanistic interpretation.

4.2. Process Dynamics

In the experiments discussed here, the processes governing polysaccharide and silica polymer growth and aggregation was deduced by fitting the data for the whole-cells (Si and Si + Fe experiments; areas for 1150–950 and 830–770 cm^{-1}) using Eqn. 3. The double logarithmic plot ($\ln[-\ln(1-\alpha)]$ vs. [ln Si-load]) in Figure 9 provides a series of pairs of straight lines corresponding to the Si and the Si + Fe experimental data.

In this study, from the least-squares regression (Fig. 9), the values for the coefficients (k_a and n) relating to the changes in absorbance of the polysaccharide or silica polymers observed

Table 3. Dynamic aggregation parameters (n and k_a) for the growth of the mixed Si-O/C-O vibrations (band 10; 1150–950 cm^{-1}) and the singular Si-O vibrations (band 12; 830–770 cm^{-1}) during the silicification of *Calothrix* sp. whole-cells in the Si (fits # 1, 3, 5) and the Si + Fe (fits # 2, 4, 6) experiments.

Fit # in Fig. 9	Aggregation coefficient, k_a (μmol^{-1} Si)	n
1 (Si: 1150–950 cm^{-1})	$K_{a,\,1\text{-}Si} = 0.41 \times 10^{-2}$	0.8
2 (Si + Fe: 1150–950 cm^{-1})	$k_{a,\,1\text{-}Si+Fe} = 2.51 \times 10^{-2}$	1.1
3 (Si: 1150–950 cm^{-1})	$K_{a,\,2\text{-}Si} = 2.36 \times 10^{-2}$	2.2
4 (Si + Fe: 1150–950 cm^{-1})	$k_{a,\,2\text{-}Si+Fe} = 2.40 \times 10^{-2}$	1.8
5 (Si: 830–770 cm^{-1})	$K_{a,\,3\text{-}Si} = 2.32 \times 10^{-2}$	3.5
6 (Si + Fe: 830–770 cm^{-1})	$k_{a,\,3\text{-}Si+Fe} = 2.33 \times 10^{-2}$	3.8

were calculated for both the Si and the Si + Fe systems (Table 3). In both systems, the observed change in slope (n) with increasing silica load indicates a change in growth and aggregation process during the silicification process. Combining these values with the microscopic and spectroscopic observations presented above (Figs. 4, 6, and 7), the processes that govern the silicification reactions can be interpreted as a two-phase process.

4.2.1. Phase 1: Cellular Response to Silicification

In the first phase, the spectra are governed by a small increase in integrated area for band 10 (mixed Si-O/C-O vibrations) indicating either the formation of additional exo-polymeric polysaccharide or the growth and aggregation of silica polymers. At these low Si-loads (4–11 and 4–7 μmol for the Si and Si + Fe experiments, respectively), no Si-O peaks were observed at 800 cm^{-1} thus supporting the hypothesis that the observed change in integrated area was solely a result of the increase in exo-polymeric polysaccharides. This hypothesis is also supported by the fact that if Si-O bonds were important their stronger ionic character would have a much larger effect on the infrared spectra. The change in spectral features is thus dominated by the effects of the growing sheath which corresponds to an increase in exo-polymeric polysaccharide concentration. This observation is also supported by qualitative microscopic evidence documenting the increase in sheath thickness in response to repeated equilibration with silica-supersaturated solutions (Phoenix et al., 2001; Benning et al., 2002).

4.2.2. Phase 2: Silica Accumulation on the Cyanobacterial Cells

The second phase (21–43 μmol) is characterized by a change in slope for both the Si-O/C-O mixed vibration (band 10) and the appearance of the singular Si-O vibration (band 12, Fig. 9). In the first case (the Si-O/C-O mixed band), this change in slope indicates a more ionic character for the formed bonds which points to a switch to pure Si-O bonds representing newly formed silica aggregates on the surface of the cyanobacterial cells. This switch is confirmed by the formation of the distinct Si-O vibration at 800 cm^{-1} (band 12) at Si-loads $>$ 11 μmol. These Si-O vibrations are the result of inorganic condensation of hydrated SiO_4 units (Perry, 1989; Perry and Keeling-Tucker, 2000). The continued formation of these SiO_4 tetrahedra at 800 cm^{-1} is believed to be solely a function of available silica (saturation state) and not due to bacterially enhanced precipitation caused by a lowering of the interfacial free energy required for precipitation.

A comparison between the Si and the Si + Fe experiments shows an insignificant difference between the two sets of experiments except in phase 1, where the increase in polysaccharide polymer in the pure Si experiments is less prominent than in the Si + Fe experiments (Table 3). This may be a consequence of the iron sorbing faster to the cyanobacteria cells, thus impeding the further growth of the sheath (Yee et al., 2003). This supports the observations of Ferris et al. (1988) and Fortin et al. (1997), who have shown that the binding of iron before silicification may enhance silicification and help preserve the morphology of cells, thus retaining them for fossilization. The above mentioned studies have suggested that although microbial cells act as a passive surface, they are necessary in the silicification process as dead cells were unable to induce the formation of particulate silica. This again would appear to suggest that cells are necessary to change the chemical equilibrium that stimulates polycondensation, however, in the second phase, the presence of iron did not affect the growth or accumulation of the silica nano-spheres and thus the derived coefficients are equal.

In the sheath spectra (Fig. 8), the same general trends were observed. At Si-loads $\geq$ 11 μmol the strong ionic Si-O bonds dominate the spectra. The formation of Si-O bonds at these Si-loads was corroborated by the appearance of the bands at 950 and 800 cm^{-1}. These bands are related to the formation of inorganic amorphous silica units.

The process observed in phase 2, leads to the formation of the nano-spherical silica particles as shown in the microphotographs (Fig. 4b). This process can be compared with inorganic or ionic low molecular weight surfactant induced silica nanospheres formation reactions (via the Stöber process, e.g., Stöber et al., 1968). Such studies showed that nucleation and growth of silica particles was dependent on the hydration level of the starting solutions or gels or the concentration of the surfactant that induced nucleation. For example, in the abiotic process when growth was induced from a 1% SiO_2 solution (with Å-size silica seeds) at slightly acidic pH conditions, the formation of 30- to 700-nm-large spherical particles occurred relatively fast with the radius growing exponentially with time (Martin, 1987). At lower silica concentrations (0.01–0.1 wt % SiO_2) and pH $\geq$ 7, the process also produced nano-spheres (10–1000 nm) but the reactions were orders of magnitude slower and the process was reaction-limited (Lin et al., 1990; Martin et al., 1990; Pontoni et al., 2002) which is similar to the process observed in this study.

In natural systems, silica biomineralization occurs usually in water at near neutral pH with silanol groups condensing from supersaturated solutions upon cooling. The kinetics of the inorganic precipitation of amorphous silica from solution has been studied and a reaction-limited mechanism with an activation energy of ~50 to 60 kJ/mol was proposed (Rimstid and Barnes, 1980; Caroll et al., 1998). In geothermal fluids the concentration of silica dissolved is commonly high enough (up to 700 ppm) for polymerization to occur spontaneously. However, where cyanobacteria are present, silica condenses on their outer layers (sheaths, capsules). Silica particles grow progres-

sively as aggregation proceeds, leading to the formation of colloidal particles, which upon further condensation of silica from the supersaturated solution grow into large aggregates.

Thus, when comparing the literature data discussed above with the results of this study it becomes evident that in the presence of the cyanobacterial filaments, the silica nano-sphere formation observed in stage 2, occurred mostly by a slow growth process and the aggregation of these nanoparticles followed a reaction-limited path.

4.3. Silicification Synopsis

The findings presented in this study provide a new interpretation for the processes leading to the silicification of cyanobacteria. The data supports a two-stage process in which the formation of nano-sized silica particles on cyanobacterial cells follows an initial thickening of the cyanobacterial sheath. In this initial phase, the formation of new hydrated polysaccharides polymers leads to the increase in thickness of the exo-polymeric polysaccharide sheath. This process is supported by independent microscopic evidence (Phoenix et al., 2001; Benning et al., 2002), showing the increase in sheath with increasing silica load. Following this initial sheath-forming stage, the process switched at higher Si-loads to a second stage, in which polymerizing silica units forming in the supersaturated aqueous environment begin to accumulate onto the 'freshly grown' microbial sheath surface. The effect of the formation of new polysaccharides will be small compared to silica aggregation, and thus the more ionic Si-O bonds will dominate the infrared spectra. Once a siloxane unit is attached to the cyanobacterial surface (via hydrogen bonds), additional Si-O bonds will form. A further increase in Si-load will lead to the formation of silica nanoparticles expressed via the formation of inorganic siloxane bonds (peak at $\sim$800 cm^{-1}). This step is governed by the growth of purely inorganic Si-O-Si bonds via the formation of an oxo bridge (Si-O-Si) while one water molecule is removed. Thus, a silica network made of corner sharing [SiO_4] tetrahedra is obtained when all Si-O groups have reacted.

4.4. Geological Applications

Much of what is understood about the evolution of early life forms comes from the examination of microbe/mineral interactions in modern hot-spring environments or Precambrian silicified microfossils and stromatolites. In each case, microbial populations are inextricably linked to silica deposition yet, what remains unresolved is whether the microbes actually exerted any control over the silicification process. In this study, based on the IR and electron microscopic evidence, it can be concluded that the *Calothrix* sp. provides an interface for silica accumulation. The microorganisms appear to respond to silicification by initially producing more sheath material, and then by allowing silica to aggregate freely on their surface. The latter process is most probably unavoidable, as it is just a response to constant exposure to a supersaturated silica solution. Thus, the suggestions that microorganisms induce and enhance the nucleation of silica from supersaturated solutions are unsubstantiated and the laboratory and field-based studies suggesting an active role of microorganisms in silica nucleation should be reinterpreted. At least for cyanobacteria, it can be concluded that their thickened exo-polymeric polysaccharide sheath surface only provides a surface for silica growth and aggregation, while simultaneously protecting the internal cell structure from detrimental biomineralization (Phoenix et al., 2000; Konhauser et al., 2001). However, perhaps this ability of cyanobacteria to create more exo-polymeric sheath represents an ancient legacy of some microorganisms growing in aqueous environments subject to high dissolved silica levels. Not surprisingly, the most ancient verifiable microfossils appear to be cyanobacterial in origin and thus the findings presented here may be applicable to those ancient settings. Certainly, the ancient oceans contained high concentrations of silica (Siever, 1992) and iron (Morris, 1993), and thus unsurprisingly many ancient microfossils are found preserved in cherts and silica stromatolites (e.g., Cloud, 1965; Awramick et al., 1983; Schopf, 1993).

The dynamic silicification data derived from the FTIR spectra combined with the microscopic evidence that the silica particles forming on the cyanobacterial surfaces are spherical in shape corroborates previous observations in naturally silicified microbial films (Schultze-Lam et al., 1995; Konhauser and Ferris, 1996; Jones et al., 1998, 1999; Konhauser et al., 1999; Mountain et al., in press) and other laboratory experiments (e.g., Oehler and Schopf, 1971; Oehler, 1976; Phoenix et al., 2000). However, this is the first direct quantification of the formation process for such nano-spheres on single cyanobacterial filaments using in situ spectroscopic and microscopic methods. The combined data suggest that in the first stage the cells react by way of producing more exo-polymeric polysaccharides. Most of the silica that eventually leads to the observed spherical aggregates forms via inorganic precipitation and thus the role of the cyanobacteria in silica nucleation is minimal. Considering that much of the silicification process is evidently inorganically controlled, it is unsurprising that microbes appear to have little effect upon silica precipitation kinetics, which is in agreement with similar batch type experiments (Yee et al., 2003; Phoenix et al., in press). In natural environments, the further addition of silica from the supersaturated geothermal waters leads to the full encrustation of the cyanobacterial filaments, their inevitable lysis and necrosis. However, new colonies will grow on the newly formed silica layers and the process will be repeated providing the means to form sinters as observed in many modern and ancient geothermal systems.

5. SUMMARY

The experimental results demonstrate that IR micro-spectroscopy can be applied to monitor cyanobacterial silicification in situ and in vivo. Spectra of silicified *Calothrix* sp. filaments indicate that the extent of silicification can be quantified as a function of sorbed Si-load. Silicified samples display a distinct increase in absorbance intensity between 1150 and 800 cm^{-1} that is interpreted as a two stage process that shows (1) the formation of new polysaccharide polymers within the cyanobacterial sheath and (2) the subsequent accumulation of silica nanospheres on the cell surface. This data was used to derive an empirical dynamic model as a function of increasing Si-load. This model identifies two distinct steps, corresponding to a biologically driven exo-polymeric polysaccharide growth followed by an inorganically controlled silica accumulation,

with the latter being the dominant process in the silicification of cyanobacterial cells. Complementary microscopic evidence showed the silicification of the cyanobacterial filaments via the formation of 20 to 200 nm silica spheres on the cyanobacterial surface. These results successfully explain field-based observations and provide a molecular-scale understanding of the role of cyanobacteria in silica precipitation reactions.

However, polysaccharide and silica polymers usually form structures of mixed or changing geometry during growth or aggregation and the Si-load dependent FTIR data do not provide any structural information. Furthermore, in heterogeneous systems like the one discussed here, an analysis based solely on an Avrami-type approach and microscopic evidence will not provide an unique solutions for the growth mechanism of both the polysaccharide and silica polymers. Only further quantification of these processes based on time resolved spectroscopic and microscopic data, will provide the information needed to fully quantify and unambiguously understand the kinetics of the microbial silicification process.

Acknowledgments—The financial support provided by the UK Natural Environment Research Council, Direct Access to Synchrotron Radiation Source grant (#37059) and by a grant from The Leverhulme Trust (Ref. #F/00122/F) are greatly acknowledged. V. Phoenix at the University of Toronto was kindly supported by Professor F. Grant Ferris through The Natural Science and Engineering Research Council (NSERC) of Canada, and through an Ontario Premier's Research Excellence Award. Dr. Eric Condliffe of the Electron Optics Laboratory in Leeds is thanked for making the high-resolution FEG-SEM pictures possible. Advice on aggregation and reaction mechanisms from Michael J. Pilling, Department of Chemistry, University of Leeds is much appreciated. The comments of the AE and of two anonymous reviewers are greatly acknowledged.

Associate editor: J. P. Amend

REFERENCES

Avrami M. (1941) Kinetics of phase change III. *J. Chem. Phys.* **9,** 177–184.

Awramik S. M., Schopf J. W., and Walter M. R. (1983) Filamentous fossil bacteria from the Archean of Western Australia. *Precam. Res.* **20,** 357–374.

Benning L. G., Phoenix V., Yee N., Tobin M. J., Konhauser K. O., and Mountain B. W. (2002) Molecular characterization of cyanobacterial cells during silicification: A synchrotron-based infrared study. *Geochem. Earth Surf.* **6,** 259–263.

Benning L. G., Phoenix V., Yee N., and Tobin M. J. (2003) Molecular characterization of cyanobacterial silicification using synchrotron infrared micro-spectroscopy. *Geochim. Cosmochim. Acta* **67,** 0000–0000.

Cady S. L. (2001) Paleobiology of the Archean. *Adv. Appl. Microbiol.* **50,** 3–35.

Cady S. L. and Farmer J. D. (1996) Fossilization processes in siliceous thermal springs: trends in preservation along thermal gradients. In *Evolution of Hydrothermal Ecosystems on Earth (and Mars?)* (eds. G. R. Brock and J. A. Goode), pp. 150–173. John Wiley, Chichester, UK.

Carroll S., Mroczek E., Alai M. and Ebert M. (1998) Amorphous silica precipitation (60 to 120 degrees C): Comparison of laboratory and field rates. *Geochim. Cosmochim. Acta* **62,** 1379–1396.

Cha J. N., Stucky G. D., Morse D. E., and Deming T. E. (2000) Biomimetic synthesis of ordered silica structures mediated by block copolypeptides. *Nature* **403,** 289–292.

Cloud P. E., Jr.. (1965) Significance of the Gunflint (Precambrian) microflora. *Science* **148,** 27–35.

Daughney C. J., Fein J. B., and Yee N. (1998) A comparison of the thermodynamics of metal adsorption onto two common bacteria. *Chem. Geol.* **144,** 161–176.

Diem M. (1993) *Introduction to Modern Vibrational Spectroscopy*. Wiley Intercience, New York.

Fein J. B., Daughney C. J., Yee N., and Davis T. A. (1997) A chemical equilibrium model for metal adsorption onto bacterial surfaces. *Geochim. Cosmochim. Acta* **61,** 3319–3328.

Fein J. B., Scott S., and Rivera N. (2002) The effect of Fe on Si adsorption by Bacillus subtilis cell walls: Insights into non-metabolic bacterial precipitation of silicate minerals. *Chem. Geol.* **182,** 265–273.

Ferris F. G., Beveridge T. J., and Fyfe W. S. (1986) Iron-silica crystallite nucleation by bacteria in a geothermal sediment. *Nature* **320,** 609–611.

Ferris F. G., Fyfe W. S., and Beveridge T. J. (1988) Metallic ion binding by *Bacillus subtilis*: Implications for the fossilization of microorganisms. *Geology* **16,** 149–152.

Fortin D., Ferris F. G. and Beveridge T. J.(1997) Surface mediated mineral development by bacteria. In *Geomicrobiology: Interactions Between Microbes and Minerals* (eds. J. F. Banfield and K. H. Nealson). Mineralogical Society of America, Washington DC.

Fowle D. A., Fein J. B., and Martin A. M. (2000) Experimental study of uranyl adsorption onto *Bacillus subtilis*. *Environ. Sci. Technol.* **34,** 3737–3741.

Francis S., Margulis L., and Barghoorn E. S. (1978) On the experimental silicification of microorganisms II. On the time of appearance of Eukaryotic organisms in the fossil record. *Precam. Res.* **6,** 65–100.

Hinman N. W. and Lindstrom R. F. (1996) Seasonal changes in silica deposition in hot spring systems. *Chem. Geol.* **132,** 237–246.

Iler R. K. (1979) *The Chemistry of Silica*. John Wiley, New York.

Iler R. K. (1980) Isolation and characterization of particle nuclei during the polymerization of silicic acid to colloidal silica. *J. Coll. Interface Sci.* **71,** 138–148.

Jones B., Renault R. W., and Rosen M. R. (1998) Microbial biofacies in hot-spring sinters: A model based on Ohaaki Pool, North Island, New Zealand. *J. Sed. Res.* **68,** 413–434.

Jones B., Renault R. W., and Rosen M. R. (1999) Actively growing siliceous oncoids in the Waiotapu geothermal area, North Island, New Zealand. *J. Geol. Soc. London* **156,** 89–103.

Kessels W. M. M., Smets A. H. M., Marra D. C., Aydil E. S., Schram D. C., and van de Sanden M. C. M. (2001) On the growth mechanism of a-Si-H. *Thin Solid Films* **383,** 154–160.

Konhauser K. O (2000) Hydrothermal bacterial biomineralization: Potential modern-day analogues for Precambrian banded iron formation. In *Marine Authigenesis: From Global to Microbial*, SEPM Special Publication (eds. C. R. Glenn, J. Lucas and L. Prévôt), **66,** 133–145.

Konhauser K. O. and Ferris F. G. (1996) Diversity of iron and silica precipitation by microbial mats in hydrothermal waters, Iceland: Implications for Precambrian iron formations. *Geology* **24,** 323–326.

Konhauser K. O., Phoenix V. R., Bottrell S. H., Adams D. G., and Head I. M. (1999) Microbial-silica interactions in modern hot spring sinter. *Geochem. Earth Surf.* **5,** 263–266.

Konhauser K. O., Phoenix V. R., Bottrell S. H., Adams D. G., and Head I. M. (2001) Microbial-silica interactions in Icelandic hot spring sinter: Possible analogues for some Precambrian siliceous stromatolites. *Sedimentology* **48,** 415–433.

Kröger N., Lehmann G., Rachel R., and Sumper M. (1997) Characterization of a 200-kDa diatom protein that is specifically associated with a silica-based substructure of the cell wall. *Eur. J. Biochem.* **250,** 99–105.

Kröger N., Deutzmann R., Bergsdorf C., and Sumper M. (2000) Species-specific polyamides from diatoms control silica morphology. *Proc. Natl. Acad. Sci. U. S. A.* **97,** 14133–14138.

Lehn J.-M. (2002) Toward self-organization and complex matter. *Science* **295,** 2400–2403.

Lin M. Y., Lindsay H. M., Weitz D. A., Ball R. C., Klein R., and Meakin P. (1990) Universal reaction-limited colloid aggregation. *Phys. Rev. A* **41** (*4*), *2005–2020.*

Leo R. F. and Barghoorn E. S. (1976) Silicification of wood. *Botan. Museum Leaflets Harv. Univ.* **25 (*1*)**, 1–29.

Licoppe C., Nissin Y. I., and Moison J. M. (1992) Surface chemistry and growth modes in the photochemical deposition of silica films. *Phys. Rev. B* **45** (*11*), *6275–6278.*

Makrides A. C., Turner M., and Slaughter J. (1980) Condensation of silica from supersaturated silicic acid solutions. *J Coll. Interface Sci.* **73,** 345–367.

Martin J. E. (1987) Slow aggregation of colloidal silica. *Phys. Rev. A* **36** (*7*), 3415–3426.

Martin J. E., Wikcoxon J. P., Schaefer D., and Odinek J. (1990) Fast aggregation of colloidal silica. *Phys. Rev. A* **41** (*8*), 4379–4391.

Morris R. C. (1993) Genetic modeling for banded iron-formation of the Hamersley Group, Pilbara Craton, Western Australia. *Precam. Res.* **60,** 243–286.

Mountain B. W., Benning L. G. and Boerema J.(in press) Experimental studies on New Zealand hot spring sinters: Rates of growth and textural development. *Can. J. Earth Sci*.

Oehler J. H. (1976) Experimental studies in Precambrian paleontology: Structural and chemical changes in blue-green algae during simulated fossilization in synthetic chert. *Geol. Soc. Am. Bull.* **87,** 117–129.

Oehler J. H. and Schopf J. W. (1971) Artificial microfossils: Experimental studies of permineralization of blue-green algae in silica. *Science* **174,** 1229–1231.

Perry C. C. (1989) Biogenic silica. In *Biomineralisation: Chemical and Biological Perspectives* (eds. S. Mann, J. Webb, and R. J. P. Williams), pp. 233–256. VCH, Weinheim.

Perry C. C. and Keeling-Tucker K. (2000) Biosilicification: The role of the organic matrix in structural control. *J. Biol. Inorg. Chem.* **5,** 537–550.

Phoenix V. R (2001) *Microbial-Biomineral Interactions and Their Significance for the Formation of Chemical Sediments*. Ph.D. dissertation, University of Leeds.

Phoenix V. R., Adams D. G., and Konhauser K. O. (2000) Cyanobacterial viability during hydrothermal biomineralization. *Chem. Geol.* **169,** 329–338.

Phoenix V. R., Konhauser K. O., Adams D. G., and Bottrell S. H. (2001) Role of biomineralization as an ultraviolet shield: Implications for Archean life. *Geology* **29,** 823–826.

Phoenix V. R., Konhauser K. O. and Ferris F. G.(in press) Experimental study of iron and silica immobilization by bacteria in mixed Fe-Si systems: Implications for microbial silicification in hot-springs. *Can. J. Earth Sci*.

Pontoni D., Narayanan T., and Rennie A. R. (2002) Time-resolved SAXS study of nucleation and growth of silica colloids. *Langmuir* **18,** 56–59.

Rees D. A. (1977) *Polysaccharide Shapes*. Chapman and Hall, London.

Rimstidt J. D. and Barnes H. L. (1980) The kinetics of silica-water reactions. *Geochim. Cosmochim. Acta* **44,** 1683–1699.

Rippka R., Deruelles J., Waterbury J. B., Herdman M., and Stainer R. Y. (1979) Generic assignments, strain histories and properties of pure cultures of cyanobacteria. *J. Gen. Microbiol.* **111,** 1–61.

Rothbaum H. P. and Wilson R. D. (1977) Effect of temperature and concentration on the rate of polymerisation of silica in geothermal waters. *Geochemistry* **218,** 37–43.

Schopf J. W. (1993) Microfossils of the early Archean Apex chert: New evidence of the antiquity of life. *Science* **260,** 640–646.

Schultze-Lam S., Ferris F. G., Konhauser K. O., and Wiese R. G. (1995) In-situ silicification of an Icelandic hot spring microbial mat: Implications for microfossil formation. *Can. J. Earth Sci.* **32,** 2021–2026.

Schwerha D. J., Orr C-S., Chen B. T., and Soderholm S. C. (2002) Direct-on-filter analysis of crystalline silica using photoacoustic Fourier transform-infrared spectroscopy. *Anal. Chim. Acta* **457,** 257–264.

Siever R. (1992) The silica cycle in the Precambrian. *Geochim. Cosmochim. Acta* **56,** 3265–3272.

Stöber W., Fink A., and Bohn E. (1968) Controlled growth of monodisperse silica spheres in the micron size range. *J. Coll. Interface Sci.* **26,** 62.

Stuart B. and Ando D. J. (1997) Biological applications of infrared spectroscopy, ACOL publication (University of Greenwich) Wiley Chichester.

Sumper M. (2002) A phase separation model for the nanopatterning of diatom biosilica. *Science* **295,** 2430–2433.

Toporski J. K. W., Steele A., Westall F., Thomas-Keprta K. L., and McKay D. S. (2002) The similated silicification of bacteria—New clues to the modes of timing of bacterial preservation and implications for the search for extraterestrial microfossils. *Astrobiology* **2** (*1*), 1–26.

Walter M. R. (1976) Hot-spring sediments in Yellowstone National Park. In *Stromatolites* (ed. M. R. Walter), pp. 489–498. Elsevier, Amsterdam, the Netherlands.

Walter M. R., Bauld J., and Brock T. D. (1972) Siliceous algal and bacterial stromatolites in hot spring and geyser effluents of Yellowstone National Park. *Science* **178,** 402–405.

Walters C. C., Margulis L., and Barghoorn E. S. (1977) On the experimental silicification of microorganisms. I. Microbial growth on organosilicon compounds. *Precam. Res.* **5,** 241–248.

Weckesser J., Hofmann K., Jürgens U. J., Whitton B. A., and Raffelsberger B. (1988) Isolation and chemical analysis of the sheaths of the filamentous cyanobacteria *Calothrix parienta* and *C. scopulorum*. *J. Gen. Microbiol.* **134,** 629–634.

Weres O., Yee A., and Tsao L. (1981) Kinetics of silica polymerization. *J. Coll. Interface Sci.* **84,** 379–402.

Westall F., Boni L., and Guerzoni E. (1995) The experimental silicification of microorganisms. *Palaeontology* **38** (*3*), 495–528.

Whitesides G. M. and Grzybowski B. (2002) Self-assembly at all scales. *Science* **295,** 2418–2421.

Yee N., Phoenix V. R., Konhauser K. O., Benning L. G., and Ferris F. G. (2003) The effect of cyanobacteria on Si precipitation kinetics at neutral pH: Implications for bacterial silicification in geothermal hot springs. *Chem. Geol.* **199,** 83–90.